

Synthesis and structure of dithizonato complexes of copper(II), antimony(III) and tin(IV)

TREVOR T. CHIWESHE^a, MARILÉ LANDMAN^b, JEANET CONRADIE^a
and KAREL G. VON ESCHWEGE^{a*}

a Department of Chemistry, PO Box 339, University of the Free State, Bloemfontein, 9300, South Africa.
Tel: 27-51-4012923, Fax: 27-51-4017295

b Department of Chemistry, University of Pretoria, Private Bag X20, Hatfield, 0028, South Africa.
Tel: 27-12-4202527, Fax: 27-12-4204687

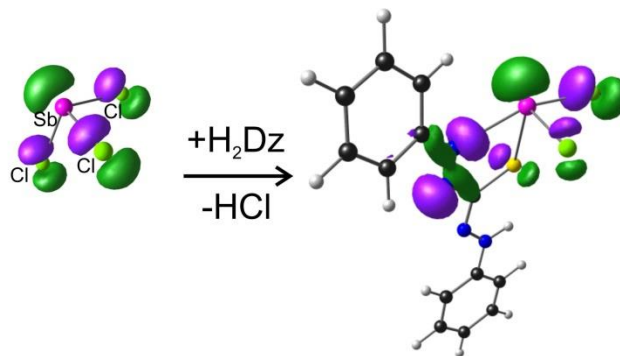
Contact author details:

Name: Karel G. von Eschwege, Tel: ++27-51-4012923, Fax: ++27-51-4017295, email: veschwkg@ufs.ac.za

Keywords

crystal, dithizone, tin, copper, antimony, DFT, orbitals, ionic radius

Graphical abstract



X-ray crystallographical data combined with DFT computational studies provide improved understanding of dithizone-metal chemistry and its observed modes of coordination.

Research highlights

- Synthesis and crystal structures of Cu^{II}, Sb^{III} and Sn^{IV} dithizonate complexes
- Coordination mode comparison with related literature examples
- DFT reaction energy calculations predict experimental products
- DFT geometries and molecular orbital renderings predict experimental products

ABSTRACT

In view of the important role of dithizone in trace metal analyses, new structural aspects and approaches used to probe metal complexes of dithizone are of interest. Three X-ray diffraction structures are reported, dichloro-*bis*(dithizonato)tin(IV), dichloro-(dithizonato)antimony(III) and *bis*(dithizonato)copper(II). During synthesis of the tin complex, autooxidation of $\text{Sn}^{\text{II}}\text{Cl}_2$ to Sn^{IV} occurred without chloride liberation. The Sb^{III} complex revealed a unique distorted seesaw geometry which is, as for the other complexes, conveniently explained by DFT calculated molecular orbital orientations. Computed lowest reaction energies are in agreement with experimentally obtained reaction products, which, together with molecular orbital renderings serve as a suitable tool towards the prediction of modes of coordination in these complexes. The S-M-N bond angle in the 5-membered coordination ring shows a linear relationship with the corresponding metal ionic radii.

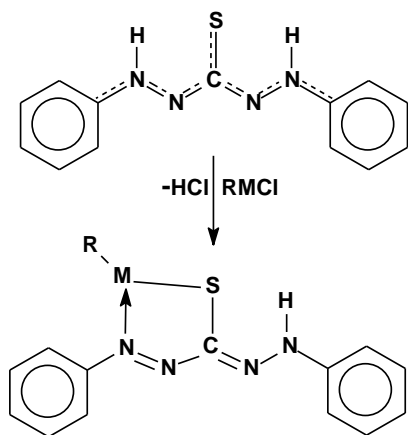
1. Introduction

In 1925 Helmuth Fischer [1] showed the great potential of dithizone (H_2Dz) for the detection and determination of heavy metal ions. Through the years it has become more or less indispensable in trace metal analysis. In 1977 Harry Irving published a thorough review on dithizone chemistry [2]. By making use of dithizone Van Staden and Taljaard [3] developed systems for the simultaneous analysis of soil and water samples containing many different metal ions. With this inexpensive technique, results comparable to that obtained by atomic absorption spectrometry were obtained. Comitre and Reis [4], also utilizing dithizone as complexing agent, achieved spectrophotometric detection limits of 12 parts per billion for the analyses of lead in plant materials. These results compare well with what may be obtained by inductively coupled plasma combined with optical emission spectroscopy (ICP-OES).

Apart from dithizone being a very important colour development reagent in trace metal analyses, as may be noted from numerous related reports published annually, it also forms the basis of the photochromic reaction observed in some metal complexes. Photo-excitation results in color-changing isomerization around the C–N bond, while the spontaneous thermal back-reaction is unaffected by light [5]. Recent femtosecond transient laser spectroscopy studies gave insight in the ultra-fast dynamics of the photochromic isomerization reaction [6].

The structures of dithizonato (HDz⁻) metal complexes are well established with a total of more than twenty X-ray data collections that have been reported up to date (see Table 3). Except for slight twists of the HDz⁻ phenyl rings in some cases, the ligand is essentially planar in all structures. A large degree of π -electron delocalization along the ligand backbone, which includes the two phenyl rings, is deduced from both experimental X-ray and theoretical density functional theory (DFT) determined bond lengths [7]. Delocalized bond lengths are longer than short double bonds and shorter than typical single bond lengths.

DFT calculations yielded structural parameters in close agreement with experimentally determined X-ray data collections [7]. Not only geometrical parameters, but also time-dependent-DFT (TDDFT) calculated oscillators (UV-visible spectra) gave good correlation with spectroscopically measured absorption bands. Both TDDFT and computed molecular orbital illustrations serve as additional means towards better understanding of structural properties in (dithizonato)metal complexes.



Scheme 1. Bidentate metal-dithizonate coordination [2]. M – metal, R – organic ligand.

HDz⁻ ligands are bidentately coordinated to the respective metals, via S and N atoms (Scheme 1). Exceptions are reported for complexes of indium, methyltin, ruthenium and osmium, where at least one HDz⁻ ligand is monodentately coordinated through sulfur [8]. Ligands are in the linear configuration. The only exception is found in an osmium cluster compound where both ligands are, due to steric reasons, in a bent configuration, i.e. 180° rotated around one C–N bond. An interesting observation here was of the dithizonato sulfur in the osmium cluster compounds being simultaneously coordinated to two adjacent metal centers, serving as a bridge between the metals.

Towards expanding the knowledge base concerned with metal-dithizonate chemistry, this study presents three new structures, clarified by applicable theoretical calculations.

2. Experimental

2.1. General

AR grade solvents (Merck) were used, without further purification. All syntheses chemicals were reagent grade and used as purchased from Sigma-Aldrich. ^1H NMR spectra were obtained on a Bruker AVANCE II 600 MHz spectrometer and data listed in the order: chemical shift (δ , reported in ppm and referenced to TMS), integral value, multiplicity and assignment.

Crystal data were collected at 150 K on a Bruker D8 Venture Kappa geometry diffractometer with duo $\text{I}\mu\text{s}$ sources, a Photon 100 CMOS detector and APEX II control software using Quazar multi-layer optics monochromated Mo- $\text{K}\alpha$ radiation by means of a combination of ϕ and ω scans. Data reduction was performed using SAINT+ and the intensities were corrected for absorption using SADABS [9]. The structures were solved by intrinsic phasing using SHELXTS and refined by full-matrix least squares using SHELXTL and SHELXL-97/2013/2014 [10]. In the structure refinement all hydrogen atoms attached to carbon atoms were added in calculated positions and treated as riding on the atom to which they are attached. All non-hydrogen atoms were refined with anisotropic displacement parameters. All isotropic displacement parameters for hydrogen atoms were calculated as $X \times U_{\text{eq}}$ of the atom to which they are attached; $X = 1.5$ for the methyl hydrogens and 1.2 for all other hydrogens. The tin complex crystallized as a twin crystal and was refined as such.

DFT calculations of this study were performed with the B3LYP [11] functional as implemented in the Gaussian 09 program package [12] utilizing the GTO def2-TZVPP basis set [13] on Sb and Sn, and 6-311G(d,p) on the other atoms. GTO (HOMO and LUMO) were visualized at the same level of theory. Calculations were also done with the PW91 (Perdew-Wang 1991) [14] GGA functional as implemented in the ADF 2013 program system [15] with the STO QZ4P basis set on Sb and Sn and TZ2P on the other atoms. Geometries of the neutral complexes were optimized in gas phase. Calculations were carried out at default temperature (298.15 K) and pressure (1 atm).

2.2. Synthesis

2.2.1. Synthesis of bis(dithizonato)copper(II) (1).

To a dark green solution of dithizone (0.31 g, 1.2 mmol) in dichloromethane (100 mL), an aqueous CuCl_2 (0.10 g, 0.76 mmol) solution (50 mL) was added and stirred for 30 minutes at room temperature. The violet organic layer was removed, washed with distilled water and filtered through anhydrous sodium sulphate. Crystals suitable for single crystal X-ray data collection were obtained by room temperature recrystallization from dichloromethane-hexane (1:1) solution.

$\text{Cu}(\text{HDz})_2$: Yield 89 %; m.p. 187 °C; UV-Vis λ_{max} (dichloromethane, nm): 441; ^1H NMR (600 MHz, DMSO-d_6 , 20 °C): δ 7.54-7.75 (20 H, m, C_6H_5), 8.22 (2 H, s, NH).

2.2.2. Synthesis of dichloro-(dithizonato)antimony(III) (2)

To a solution of dithizone (0.50 g 2.0 mmol) in dichloromethane (100 mL), a methanolic SbCl_3 (0.49 g, 2.1 mmol) solution (100 mL) was added and stirred for 30 minutes at room temperature, a deep red solution forming. The solvent was removed under reduced pressure. The product was dissolved in dichloromethane (leaving excess salt undissolved) and filtered through sodium sulphate. Green crystals, suitable for single crystal X-ray data collection, were obtained by room temperature recrystallization from dichloromethane-hexane (1:1) solution.

$\text{Sb}(\text{HDz})\text{Cl}_2$: Yield 93 %; m.p. 204 °C; UV-Vis λ_{max} (dichloromethane, nm): 501; ^1H NMR (600 MHz, DMSO-d_6 , 20 °C): δ 7.15-7.92 (11 H, m, C_6H_5 and NH).

2.2.3. Synthesis of dichloro-bis(dithizonato)tin(IV) (3)

To a solution of dithizone (0.50 g; 2.0 mmol) in dichloromethane (100 mL) an aqueous $\text{SnCl}_2 \cdot 2\text{H}_2\text{O}$ (0.25 g, 1.1 mmol) solution (50 mL) was added and stirred for 30 minutes at room temperature. The violet organic layer was removed, washed with distilled water and filtered through anhydrous sodium sulphate. Crystals suitable for single crystal X-ray data collection were obtained by room temperature recrystallization from dichloromethane-hexane (1:1) solution.

$\text{Sn}(\text{HDz})_2\text{Cl}_2$: Yield 88 %; m.p. 228 °C; UV-Vis λ_{max} (dichloromethane, nm): 518; ^1H NMR (600 MHz, DMSO-d_6 , 20 °C): δ 6.99-7.82 (20 H, m, C_6H_5), 7.93 (2 H, s, NH).

3. Results and Discussion

3.1. *Crystallographic Structures*

The crystal structures of **1 - 3** are shown in Figure 1. These Ortep drawings [16], with anisotropic displacements parameters at 50% probability level, also show the numbering system. Crystallographic and refinement data is listed in Table 1. The crystal data, data collection, structure solution and refinement details are available in each CIF, as also deposited to the Cambridge Crystallographic Database (CCDC deposition numbers 1404517-1404519). Selected structural parameters are summarized in Table 2.

Table 1. Crystallographic and refinement data for **1-3**.

	1	2	3
Empirical formula	C ₂₆ H ₂₂ Cu ^{II} N ₈ S ₂	C ₁₃ H ₁₁ Cl ₂ N ₄ S Sb ^{III}	C ₂₆ H ₂₂ Cl ₂ N ₈ S ₂ Sn ^{IV}
Formula weight (g mol ⁻¹)	574.17	447.97	700.22
Temperature (K)	150(2)	150(2)	150(2)
Radiation type, λ (Å)	0.71073	0.71073	0.71073
Crystal system,	Triclinic	Monoclinic	Monoclinic
Space group	P -1	P 2 ₁ /n	P 2 ₁
a (Å)	a = 4.1619(2)	a = 13.7180(6)	a = 13.4532(8)
b (Å)	b = 10.9321(6)	b = 7.9824(4)	b = 15.4379(9)
c (Å)	c = 13.4619(7)	c = 14.3384(6)	c = 13.5657(8)
α (°)	α = 91.1290(10)	α = 90	α = 90
β (°)	β = 95.3670(10)	β = 95.8870(10)	β = 94.573(2)
γ (°)	γ = 95.6960(10)	γ = 90	γ = 90
Volume (Å ³)	606.54(5)	1561.81(12)	2808.5(3)
Z	1	4	4
D _{calc} (Mg/m ³)	1.572	1.905	1.656
Absorption coefficient (mm ⁻¹)	1.107	2.239	1.282
F(000)	295	872	1400
Crystal size (mm ³)	0.434 x 0.248 x 0.078	0.203 x 0.184 x 0.088	0.218 x 0.188 x 0.139
Theta range for data collection (°)	2.378 to 39.606	2.169 to 40.405	2.002 to 39.951
	-7≤h≤7, -19≤k≤19,	-25≤h≤25, -14≤k≤14,	-24≤h≤24, -27≤k≤27,
Index ranges	-24≤l≤24	-26≤l≤26	-24≤l≤24
Reflections collected	45949	135929	235255
R(int)	7323 [R(int) = 0.0619]	9912 [R(int) = 0.0642]	34588 [R(int) = 0.1265]
Completeness to theta = 25.242°	99.9 %	100.0 %	100.0 %
Max. and min. transmission	0.7477 and 0.5568	0.7479 and 0.6463	0.7479 and 0.5556
Refinement method	Full-matrix least-squares on F ²	Full-matrix least-squares on F ²	Full-matrix least-squares on F ²
Data used / restraints / parameters	7323 / 0 / 169	9912 / 0 / 190	34588 / 1 / 703
Goodness-of-fit on F ²	1.102	1.064	1.009
	R1 = 0.0407	R1 = 0.0304	R1 = 0.0476
Final R indices [I>2σ(I)]	wR2 = 0.1047	wR2 = 0.0574	wR2 = 0.0836
Largest diff. peak and hole (e.Å ⁻³)	1.222 and -0.393	2.160 and -0.993	1.437 and -0.653

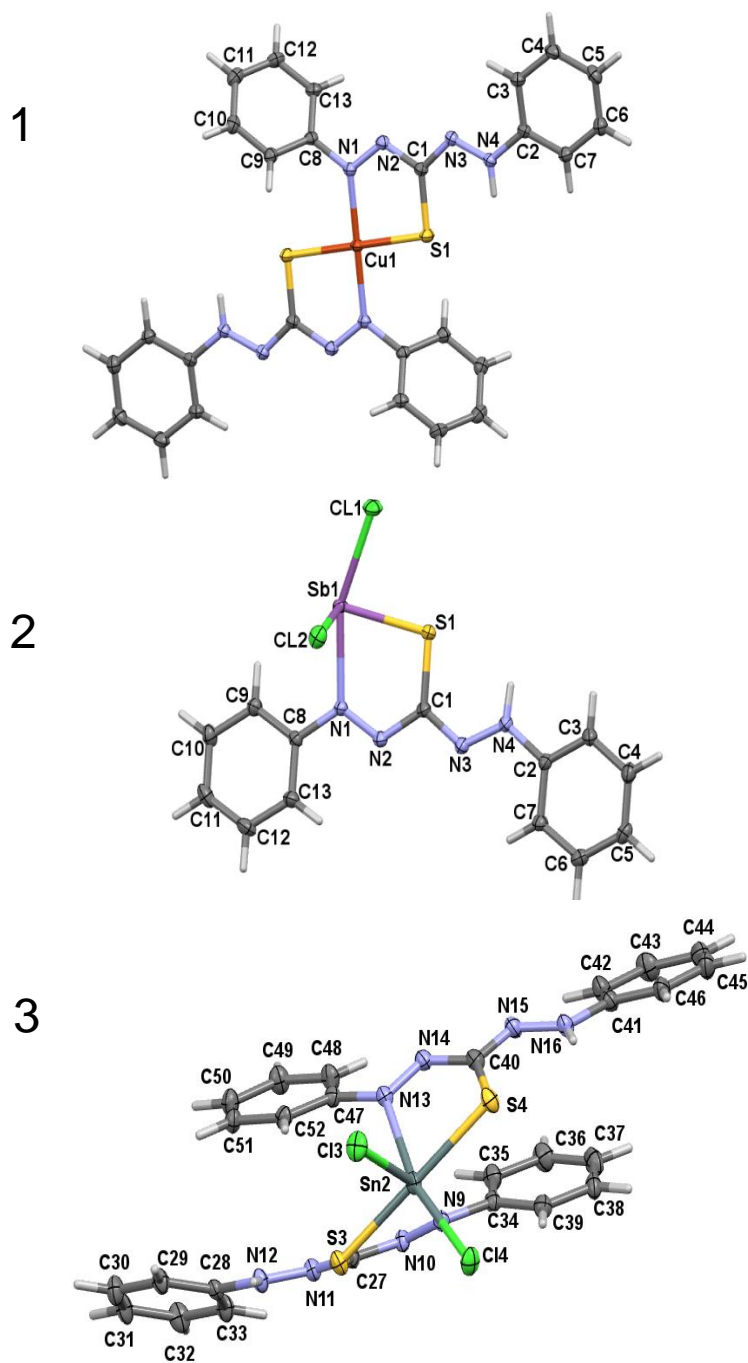


Figure 1. Perspective views (ORTEP) of $\text{Cu}(\text{HDz})_2$ (**1**), $\text{Sb}(\text{HDz})\text{Cl}_2$ (**2**) and $\text{Sn}(\text{HDz})_2\text{Cl}_2$ (**3**). Thermal ellipsoids are drawn at 50% probability level.

The structure of **1** (1961) is available in the Cambridge Crystallographic database but has no coordinates included [17]. Cell parameters are reasonably similar to what is reported in this study. Complex **1** has a square planar geometry around the Cu(II) metal ion. Two dithizonato ligands are coordinated to the metal in a *trans* configuration. The formation of a five-membered ring (Cu1-S1-C1-N2-N1) in the square planar geometry reduces the otherwise expected 90° S1-Cu1-N1 angle to 84.1°. The C8-N1-N2-C1-N3-N4-C2 molecular backbone has an extended planar conformation of sp²-hybridized nitrogen atoms. This planarity is extended to include phenyl ring C2-C7 (deviation from planarity 7.4°) and the metal ion (deviation from planarity 4.3°). However, phenyl ring C8-C13 is distorted from this plane by 45.6°, which may be the result of packing forces (see Figure 2a). Intermolecular short contacts between N2 and C13 (3.086 Å) and N2 and H13 (2.722 Å) may result in the observed deviation from planarity for C8-C13. The structure resembles the literature example of *bis*(dithizonato)nickel(II) – this square planar complex being isostructural to **1** [18]. Both complexes crystallize in the P-1 space group, with distances of 3.83 Å (²⁸Ni^{II}) and 3.37 Å (²⁹Cu^{II}) between the respective metals and the nearest atoms (sulphur) in neighbouring planes. The ³⁰Zn^{II} dithizonato complex displays a distorted tetrahedral geometry instead [19].

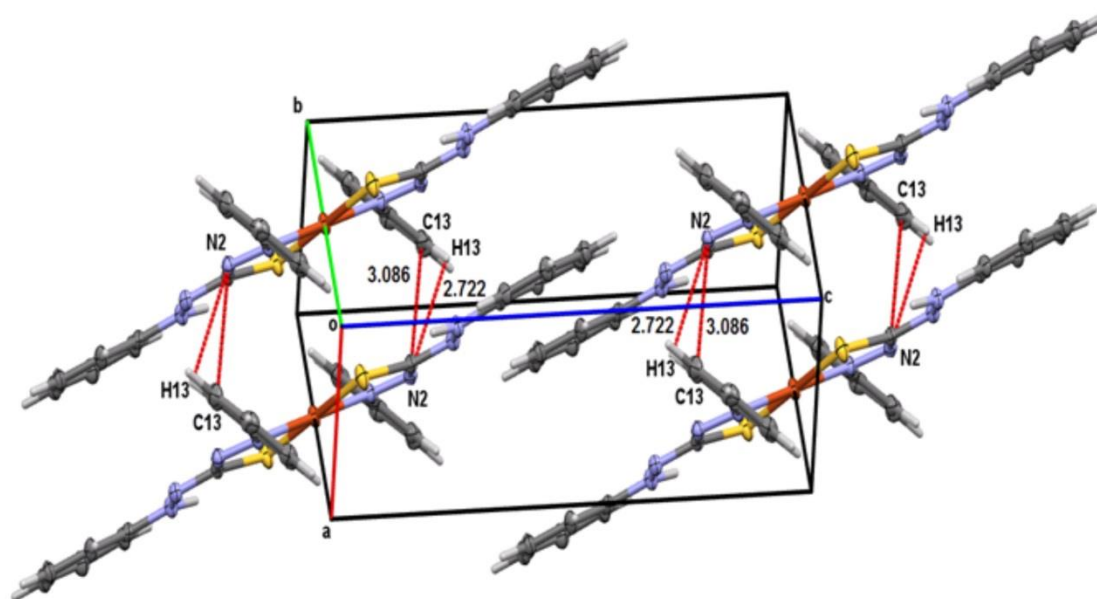
In complex **2** a distorted see-saw geometry is seen around the Sb(III) ion (Figure 1, **2**). Alternatively, it may be described as a distorted square pyramidal geometry of which one base corner is unoccupied (coordination number 4). This geometry is related to a completed square pyramidal geometry (coordination number 5) as seen in a literature example where Sb(III) is, as in **2**, again coordinated by two chlorides, but this time by a *tridentate* N,N,S-ligand, as opposed to the *bidentate* N,S-dithizonato ligand [20]. As opposed to centrally occupied positions in most other metal complexes, in both the above structures antimony occupies a peripheral position, i.e. at the centre of the pyramid base. Ligand-metal-ligand coordination angles deviate at most by *ca* 10° from 90°. The Sb metal ion is otherwise included in the planarity of the HDz- ligand, with the S1-Sb1-N1-N2 torsion angle being only 8.5°. The phenyl rings deviate only 4.6 and 14.2°, respectively, from this plane.

Complex **3** has a distorted octahedral geometry around the Sn(IV) metal centre (Figure 1, **3**). As in the copper complex, two dithizonato ligands are coordinated to the metal, with sulphur atoms in *trans* configuration, but here with the two chlorides still intact. The two molecules in the asymmetric unit are closely packed with an *intermolecular* distance of 3.347 Å between the centroids defined by phenyl rings C2-C7 and C47-C52 (Figure 2b). This distance is comparable

to *intramolecular* distances of *ca* 3.3 Å between the backbones of the two dithizonate ligands in each molecule.

The phenyl rings deviate by 1.23 to 31.54° from planarity of the extended framework. The metallocyclic angle (S-Sn-N) varies from 75.9 to 76.1°. Several Sn(IV) dithizonato complexes are known of which all contain only one dithizonato ligand, except di-*n*-butyl-*bis*(dithizonato)tin(IV) [21]. The latter distorted octahedral complex has the two HDz⁻ ligands in a square planar arrangement in the equatorial plane, while the two *n*-butyl groups are *trans* to one another in the axial positions. Also, similar coordinating atoms, e.g. the sulphurs of the HDz⁻ ligands, were found to be *cis* to one another, as opposed to what is seen in complex **3**.

1



3

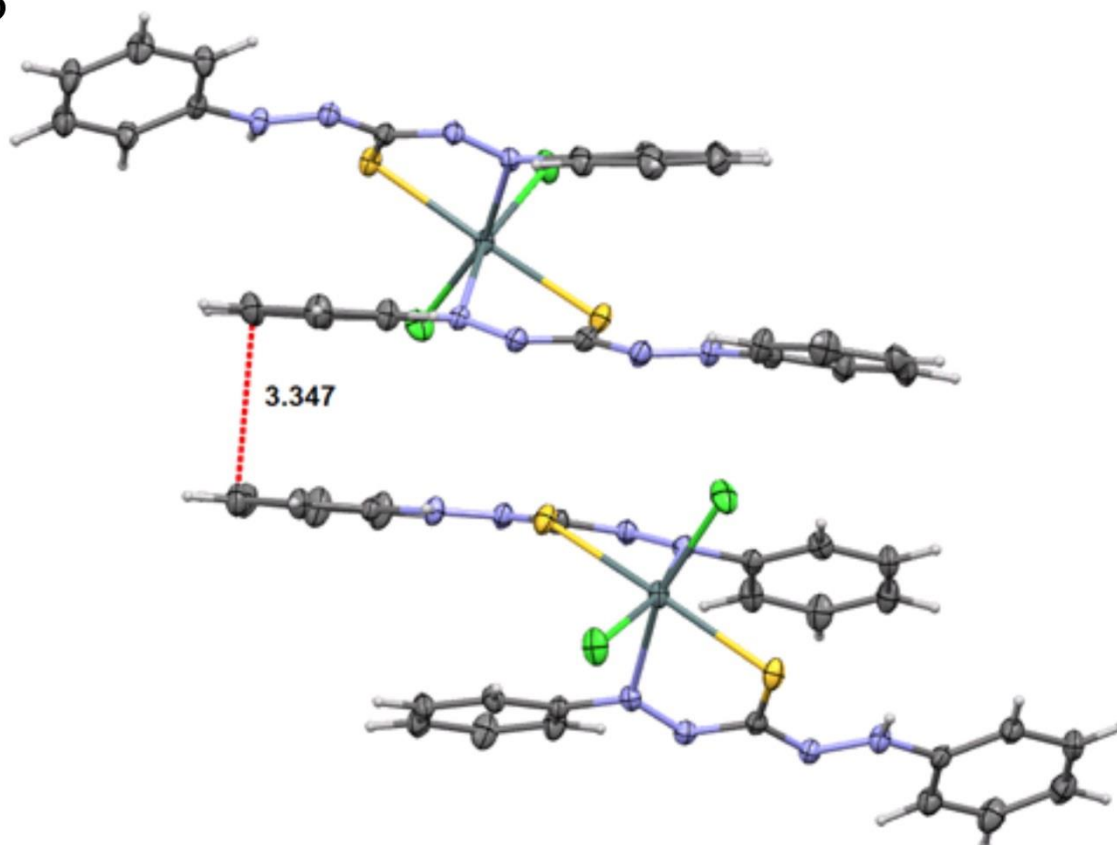


Figure 2. Intermolecular distances between the two molecules in the asymmetric unit of $\text{Cu}(\text{HDz})_2$, **1**, and $\text{Sn}(\text{HDz})_2\text{Cl}_2$, **3**.

Table 2. Selected geometric parameters for **1 – 3**

Complex	1	2	3
Bond distance (Å)			
M-S (average)	2.2890(3)	2.4297(4)	2.4636(11)
M-N (average)	2.0282(8)	2.3642(12)	2.329(3)
S1-C1	1.7391(10)	1.7620(14)	1.754(4) ^a
N1-N2	1.2792(12)	1.2760(17)	1.281(4) ^a
C1-N2	1.3694(13)	1.3629(18)	1.365(5) ^a
C1-N3	1.3217(13)	1.3186(18)	1.322(5) ^a
N3-N4	1.3184(12)	1.3096(18)	1.308(4) ^a
		2.5460(4)/	
M-Cl (average)	-	2.3749(4) ^b	2.3966(10) ^a
Bond angle (°)			
S1-M-N1	95.93(2)	75.64(3)	75.97(8) ^a
S1-M-Cl1	-	82.970(13)	90.20 (4) ^a
S1-M-Cl2	-	97.476(14)	95.96(4) ^a
S1-M-S2	-	-	170.29(3) ^a
N1-M-Cl1	-	157.36(3)	163.03(8) ^a
Cl1-M-Cl2	-	92.329(14)	95.70(4)/ 96.74(4) ^b
Torsion angle (°)			
S1-M-N1-N2	7.7(1)	11.2(1)	-27.3(2)
			144.7(2)
			27.6(2)
			27.9(2)
N1-N2-C1-N3	-175.30(8)	177.39(13)	172.4(3)
			-170.6(3)
			172.1(3)
			172.3(3)

^a Average of corresponding bonds in both molecules^b Two values differ significantly

Table 3. Comparison of selected properties of HDz⁻ crystal structures **1 - 3** with literature examples.^a

Metal Complex, HDz ⁻ coordination mode	Geometry ^c (around M)	S-M-N bond angle / °	M-S bond distance / Å	M-N bond distance / Å	M ⁿ⁺ ionic radii / pm
Au(HDz)LCI ^b [22] <i>1 x N,S-donor bidentate ligand</i>	square planar	83.83	2.249	2.131	
Bi(HDz)₃ [23] <i>3 x N,S-donor bidentate ligands</i>	octahedral	68.86	2.607	2.678	117
Co(HDz)₃ [24] <i>3 x N,S-donor bidentate ligands</i>	octahedral	84.79	2.239	1.979	69
Cu(HDz)₂ <i>2 x N,S-donor bidentate ligands</i>	square planar	84.07	2.289	2.028	71
Hg(HDz)Ph [25] <i>1 x N,S-donor bidentate ligand</i>	trigonal	73.77	2.372	2.651	110
In(HDz)₃ [26] <i>1 x S-donor monodentate ligand</i> <i>2 x N,S-donor bidentate ligands</i>	trigonal bipyramidal	77.51	2.477	2.370	94
Ni(HDz)₂ [18] <i>2 x N,S-donor bidentate ligands</i>	square planar	86.25	2.192	1.871	63
Ru(HDz)₂(bpy)₂ [27] <i>2 x S-donor monodentate ligands</i>	octahedral	— ^d	2.414	—	
Ru(HDz)O₂SL [8] <i>1 x N,S-donor bidentate ligand</i>	octahedral	79.99	2.408	2.191	
Sb(HDz)Cl₂ <i>1 x N,S-donor bidentate ligand</i>	see-saw	75.64	2.430	2.364	90
Sn(HDz)₂L₂ [28] <i>2 x N,S-donor bidentate ligands</i>	octahedral	69.93	2.492	2.674	
Sn(HDz)Ph₃ [29] <i>1 x N,S-donor bidentate ligand</i>	trigonal bipyramidal	70.13	2.446	2.734	
Sn(HDz)Me₃ [8] <i>1 x S-donor monodentate ligand</i>	tetrahedral	—	1.7619	—	
Sn(HDz)₂Cl₂ <i>2 x N,S-donor bidentate ligands</i>	octahedral	76.03	2.463	2.331	83
Tl(HDz)Ph₂L [30] <i>1 x N,S-donor bidentate ligand</i>	trigonal bipyramidal	70.17	2.648	2.622	
Pt(HDz)LL'L'' ^b [31] <i>1 x N,S-donor bidentate ligand</i>	square planar	82.06	2.270	2.145	
Zn(HDz)₂ [19] <i>2 x N,S-donor bidentate ligands</i>	tetrahedral	86.12	2.256	2.073	74

^a Literature data from ConQuest version 1.17, Copyright CCDC 2014

^b L – monodentate ligand, LL'L'' – tridentate ligand

^c Most geometries are distorted

^d Not applicable to monodentate ligands

With the exception of crystal structures of the most similar compounds, all metal dithizonate structures reported to date are represented in Table 3. As may be seen, only bismuth, cobalt and indium are *tris*-coordinated, while *uni*-coordinated complexes mostly form where some ligands already bound to the central metal are not displaced by additional incoming dithizonate ligand, as also reported here for antimony.

Whether ligands coordinate *mono-* or *bidentately*, is mainly determined by steric crowding around the metal centre, as may be seen in the ruthenium and trimethyltin complexes. The limited number of available coordination sites on the metal, as in the indium complex, prevents a N→In dative covalent bond in the 3rd *monodentate* ligand. However, the crystal structure of complex **3**, amongst others, show that bidentate ligation appears most common in tin(IV) complexes. No instances are as yet known where coordination is only through a ligand nitrogen; instead, the negative charge located mainly on the sulphur atom of the singly deprotonated ligand is the preferred site for metal coordination.

A significant increase in S-M-N bond angle sizes is observed in the 5-membered bidentate ligand rings, i.e. from as little as 68.9° in the *tris*-coordinated Bi(HDz)₃ complex to as large as 84.8° in the similarly coordinated Co(HDz)₃ complex, and even 86.3° in the Ni(HDz)₂ complex – an overall difference of 17.4°. Clearly, this variation is not attributed to steric crowding, but to differences in ionic radii of the metals. Smaller metal ion radii results in shorter metal-ligand bond distances, with closer proximity of the ligand backbone. The consequence is opening of the S-M-N bond angle, explaining the larger bond angles in event of smaller ionic radii. Figure 3a illustrates the roughly linear relationship between ionic radii and S-M-N bond angles, as well as S-M and N-M bond distances, in Figure 3b. The ionic radii which are utilized here, as listed in Table 3, correspond to related coordination geometries around each metal, i.e. either 6-coordinate octahedral or 4-coordinate tetrahedral or square planar [32]. An excellent correlation with R² = 0.97 between metal ionic radii and especially the N→M dative covalent bond lengths is seen.

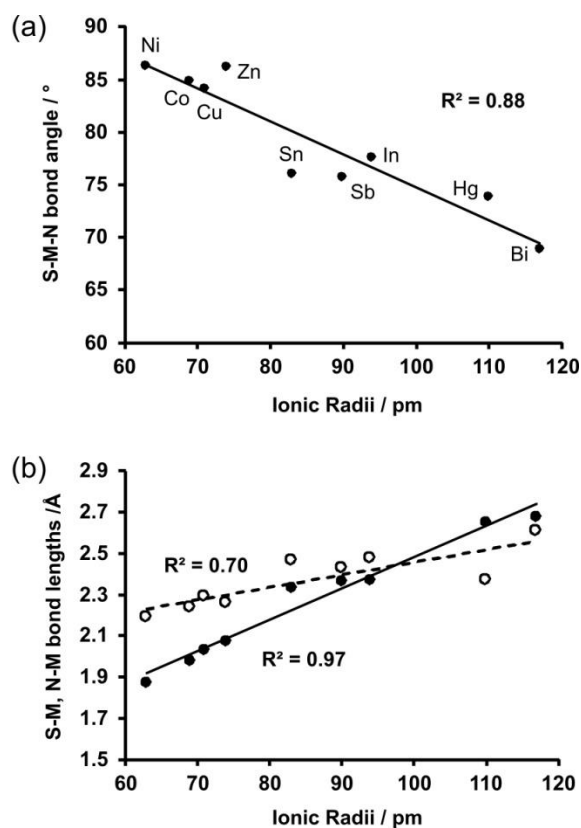


Figure 3. Ionic radii versus (a) S—M—N bond angles and (b) S—M (---) and N—M (—) bond distances. Data point labels in (a) correspond vertically to data points in (b).

Lastly, it is interesting to note the change that occurs at an ionic radius of *ca* 100 picometer (Figure 3b, *trendline intersection*). Although still increasing in bond length, at the larger atomic radii of Hg^{II} and Bi^{III} the S—M bond lengths are getting shorter than N—M bond lengths, as opposed to at radii of less than 100 pm. This observation may be explained in terms of directionality of bonding orbitals on the ligand S and N atoms involved during coordination. Considering Figure 1 (complex **1**) it may be seen that a smaller metal ion may fit more readily into the coordination space allowed by the N1—N2=C1—S1 crescent, and thus able to come into closer proximity of the bonding electron pair on N1. Bonding around this sp^2 hybridized N is strictly trigonal planar. Bond orientation on the S atom is however less rigid, as the C—S single bond may freely rotate. It follows that larger metal ions, while being prevented to getting into closer proximity of N1, is hereby allowed stronger bonding with S. This is indeed seen with especially Hg (Figure 3b), where the S—M bond distance in fact decreased on going from the smaller Sn^{IV} (2.463 Å, 83 pm), to the

much larger Hg^{II} ion (2.372 Å, 110 pm). At the same time the N–M bond distance increased by 0.32 Å.

3.2. DFT Studies

During syntheses of the dithizonato Cu^{II}, Sb^{III} and Sn^{IV} complexes, both chloride ions were substituted by HDz⁻ ligands in Cu^{II}Cl₂, while in Sb^{III}Cl₃ only one chloride was substituted. Although two HDz⁻ ligands coordinated to tin in Sn^{II}Cl₂, no chlorides were substituted, instead the oxidation state of Sn changed from II to IV. The latter agrees with the observed behavior of cobalt where, regardless of reaction reagent ratio, three dithizonato ligands always coordinate to Co^{II}Cl₂, accompanied by an oxidation state change from II to III [24]. In both cases auto-oxidation is ascribed to exposure to atmospheric oxygen, without sacrifice of ligands.

Towards explanation of the above observations DFT calculations were performed to calculate the energy changes that occur during possible syntheses reactions. B3LYP and PW91 calculations of the electronic energies (E) of the reactions gave similar results. Towards additional validation of results reaction free energies (G) were also calculated, using PW91. The computational results are summarized in Table 4.

Table 4. DFT calculated electronic (E) and Gibbs free (G) energy (eV) changes for the indicated reactions. Energies of the most favourable (lowest energy) reactions are indicated in bold.

Reaction	B3LYP	PW91	PW91	
	ΔE	ΔE	ΔG	
CuCl ₂ + H ₂ Dz → Cu(HDz)Cl + HCl	-1.174	-0.728	-0.738	
CuCl ₂ + 2H ₂ Dz → Cu(HDz) ₂ + 2HCl	-1.216	-0.518	-0.431	crystal
SbCl ₃ + H ₂ Dz → Sb(HDz)Cl ₂ + HCl	0.152	0.275	0.293	crystal
SbCl ₃ + 2H ₂ Dz → Sb(HDz) ₂ Cl + 2HCl	1.056	1.220	1.364	
SbCl ₃ + 3H ₂ Dz → Sb(HDz) ₃ + 3HCl	1.093	1.370	^a	
SnCl ₂ + 2H ₂ Dz → Sn(HDz) ₂ Cl ₂ + H ₂	-0.324	-0.972	-0.310	crystal
SnCl ₂ + 3H ₂ Dz → Sn(HDz) ₃ Cl + H ₂ + HCl	0.445	-0.136	^a	
SnCl ₂ + 4H ₂ Dz → Sn(HDz) ₄ + H ₂ + 2HCl	1.338	0.790	^a	

^a Due to the size and the high electronic energy of the indicated molecules, no frequency analysis was done here, i.e. no ΔG calculated.

For the Cu^{II}Cl₂ + nH₂Dz reaction, energy calculations showed that two products are possible; both Cu(HDz)Cl and Cu(HDz)₂. Cu(HDz)₂ was however experimentally obtained, which is in

agreement with especially the B3LYP DFT calculated related ΔE value of -1.216 eV for this reaction. The 2:1 ratio of dithizone:CuCl₂ during synthesis drives the reaction to completion, substituting both chlorides. In the Sb^{III}Cl₃ + nH₂Dz reaction, it is noted that the reaction which experimentally yielded Sb(HDz)Cl₂ also has the lowest theoretical ΔE and ΔG values by far, and thus the only product expected, even in the presence of an excess of dithizone. ΔE (B3LYP) was calculated to be 0.152 eV, as compared to more than 1 eV for complexes with potentially more than one HDz- ligand. The same was found for the Sn^{II}Cl₂ + nH₂Dz reaction, where the reaction leading to Sn^{IV}(HDz)₂Cl₂ is energetically favored compared to the other two possible reactions, i.e. with potentially three (two N,S-donor *bidentate* and one S-donor *monodentate*) or even four (two N,S-donor *bidentate* and two S-donor *monodentate*) dithizonato ligands.

To aid in the understanding of the different coordination modes of the dithizonato-metal molecules presented in this study, the frontier orbitals of the reactants and products were evaluated. Computational results show that the gas-phase DFT calculated structure of CuCl₂ is linear (Figure 4a). It is known that the solid state Cu^{II}Cl₂ structure contains corrugated sheets of distorted Cu^{II}Cl₆ octahedra with four Cu-Cl equatorial bonds (2.263 Å) and two much longer Cu-Cl apical bonds (2.991 Å) [33]. Each Cu^{II}Cl₆ octahedron shares chloride atoms with neighboring octahedra in such a way that the empirical formula of the structure is Cu^{II}Cl₂. The experimental Cl-Cu-Cl angle is 180°, which is in agreement with the gas-phase DFT calculated structure of CuCl₂. The experimental intermolecular Cu-Cu distance is 3.826 Å, see Figure 4e. Directional π -orbitals on the chlorides are responsible for the observed linear geometry in CuCl₂.

In the case of the dithizonate complex, both chlorides are substituted during reaction with HDz- to form Cu(HDz)₂. The packing of the solid state structure of Cu(HDz)₂ shows remarkable resemblance to that of CuCl₂, see Figures 4e and f. The packing of Cu(HDz)₂ molecules are arranged in sheets with a Cu-Cu intermolecular distance of 4.162 Å, which is only 0.336 Å more than in the corresponding salt crystal. The high degree of π -electron delocalization along the dithizonate backbone is responsible for its typical planar geometry, which in turn allows the observed closely packed sheets of square planar molecules. Every Cu atom in Cu(HDz)₂ has four equatorial bonds *viz.* two Cu-N bonds of 2.028 Å, and two Cu-S bonds of 2.289 Å.

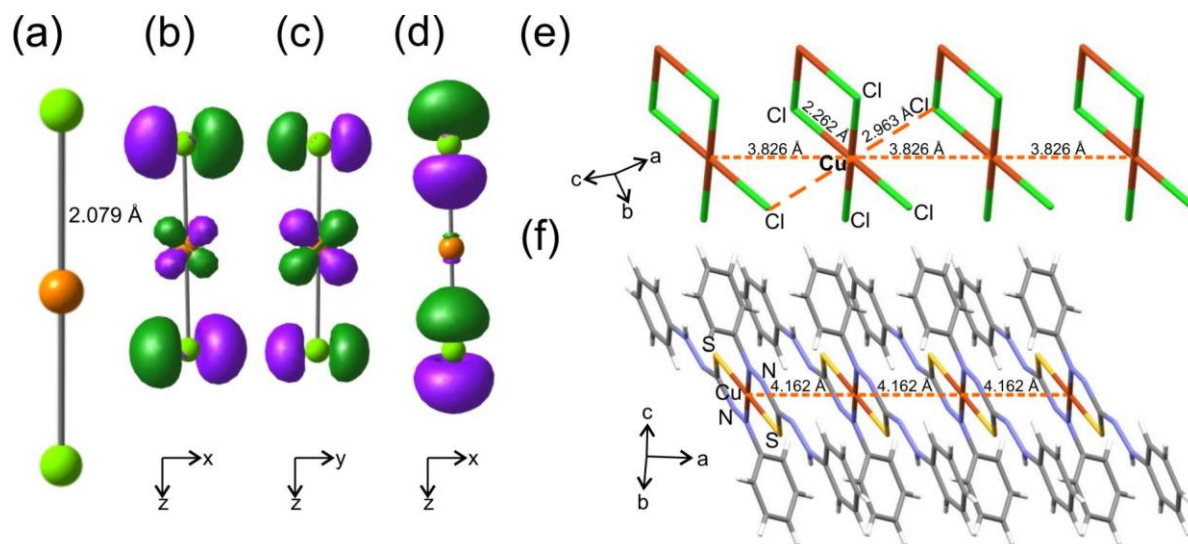


Figure 4. (a) DFT gas-phase calculated structure, selected frontier orbitals (b) STO HOMO, (c) LUMO and (d) HOMO-9 of CuCl_2 . (e) Packing diagram of the X-ray solid state structure of CuCl_2 and (f) $\text{Cu}(\text{HDz})_2$, **1**.

The arrows indicate the three units cell directions. Molecular orbital plot contours: 80 e/nm^3 . Atom colour code: Cu (orange), C (grey), Cl (green), S (yellow), N (violet) and H (white).

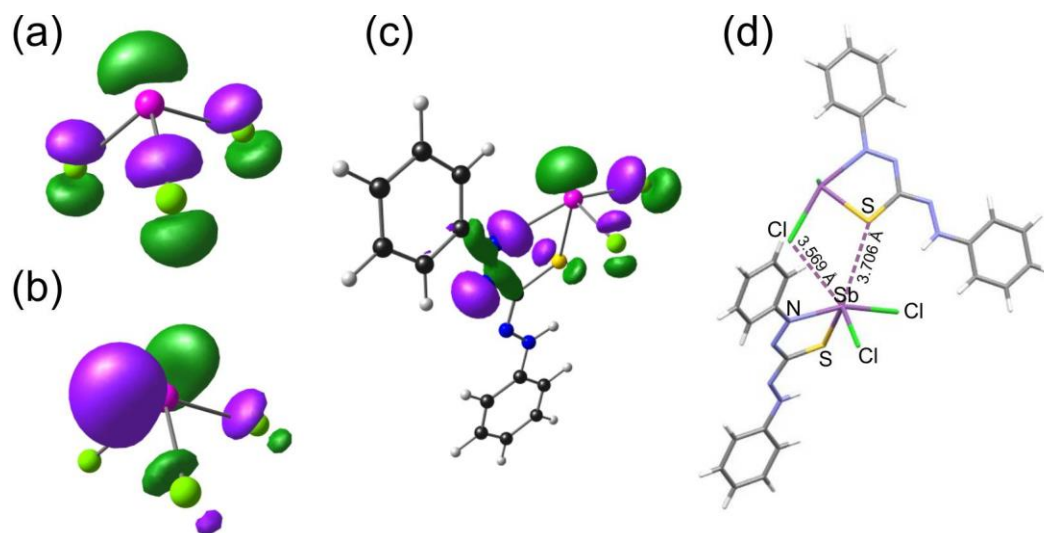


Figure 5. (a) DFT gas-phase calculated HOMO and (b) LUMO of the optimized structure of SbCl_3 . (c) HOMO-1 and (d) X-ray solid state partial packing diagram of $\text{Sb}(\text{HDz})\text{Cl}_2$.

Molecular orbital plot contours: (a) and (b) 80 e/nm^3 , and (c) 60 e/nm^3 .

Atom colour code: Sb (magenta), C (grey), Cl (green), S (yellow), N (violet) and H (white).

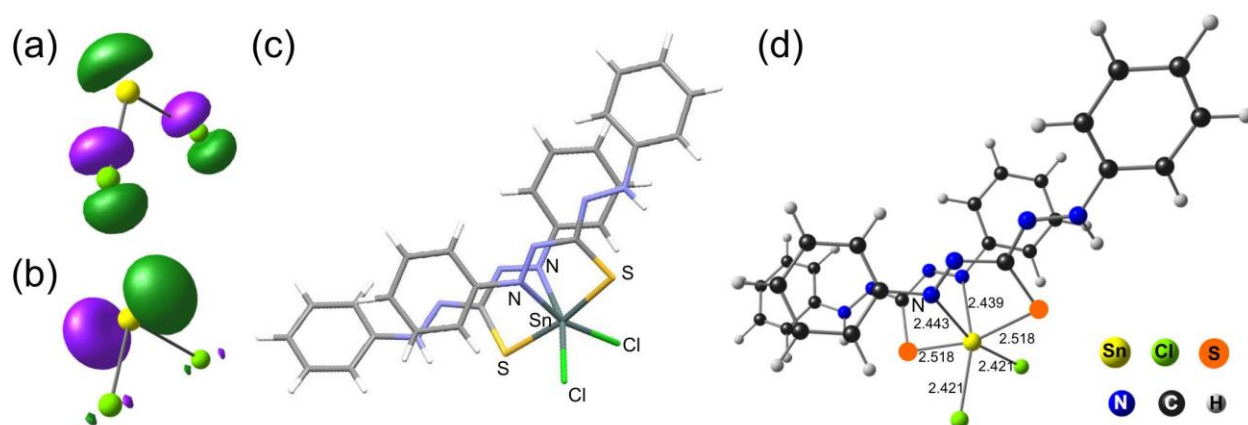


Figure 6. (a) DFT gas-phase calculated HOMO and (b) LUMO of the optimized structure of SnCl₂. (c) Experimental X-ray solid state structure and (d) the DFT (B3LYP) optimized structure of SnCl₂(HDz)₂. Selected bonds are indicated in Å. Molecular orbital plot contours: 80 e/nm³.

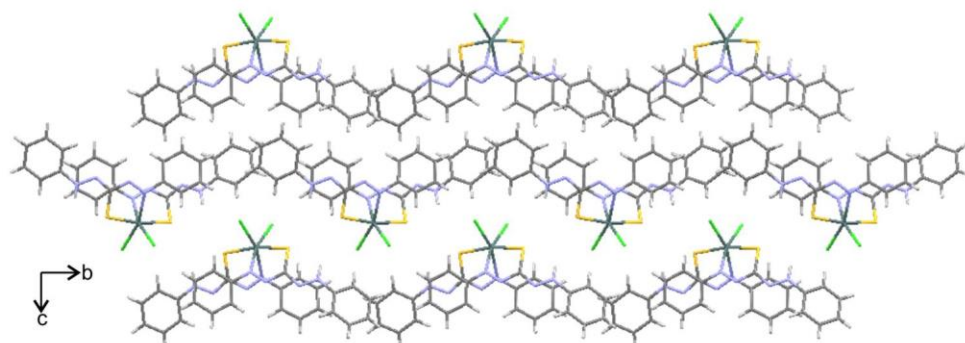


Figure 7. X-ray solid state packing of Sn(HDz)₂Cl₂. The arrows indicate the units cell directions. Atom colour code: Sn (dark grey), C (grey), Cl (green), S (yellow), N (violet) and H (white).

HOMO as well as LUMO orientations on central metals play a large role in determining coordination geometry, as is graphically illustrated by theoretically calculated molecular orbital renderings of complexes **1** – **3** in Figures 4 to 6. Additional instances here of are seen in the *tetrahedral* geometry of Zn^{II}(HDz)₂, as opposed to the *square planar* geometries of the Cu^{II}(HDz)₂ complex **1**, and Ni^{II}(HDz)₂.

The DFT gas phase optimized SbCl₃ structure is trigonal pyramidal, see Figure 5. The highest occupied molecular orbital (HOMO) shows the lone pair electrons on Sb (Figure 5a, green), while

the lowest unoccupied molecular orbital (LUMO) has an empty p-orbital on the metal (Figure 5b). During reaction with dithizone, only one Cl^- is substituted, releasing HCl . The electron lone pair on the S of HDz^- coordinates with the LUMO p-orbital on Sb (Figure 5b), resulting in a disphenoidal or seesaw type molecular geometry around Sb in $\text{Sb}(\text{HDz})\text{Cl}_2$. In the solid state packing of $\text{Sb}(\text{HDz})\text{Cl}_2$ intermolecular bonds between the HOMO-1 lone pair electrons on Sb (Figure 5c) and the Cl and S of a neighboring molecule is observed (Figure 5d, dotted lines), resulting in a pseudo-octahedral arrangement around Sb, similar to the pseudo-octahedral experimentally measured $\text{Sn}(\text{HDz})_2\text{Cl}_2$ structure (Figure 6c).

While CuCl_2 has a linear structure, the lone pair of electrons on SnCl_2 leads to a bent conformation in the gas phase. Figure 6a shows the DFT optimized structure of SnCl_2 . The bent structure of $\text{Sn}^{\text{II}}\text{Cl}_2$ is preserved when it is oxidized to $\text{Sn}^{\text{IV}}\text{Cl}_2^{2+}$ during reaction with two H_2Dz molecules, resulting in a pseudo-octahedral arrangement around Sn, see Figure 6c and d for crystal and DFT optimized structures of $\text{Sn}(\text{HDz})_2\text{Cl}_2$. The packing of $\text{Sn}(\text{HDz})_2\text{Cl}_2$ along the crystallographic a-axis shows linear arrays of molecules with metal fragments orientated towards one another while the organic part of the molecule is layered together (Figure 7).

4. Conclusions

Dithizone is extensively used as color-development reagent in trace metal analyses during which the metal to ligand ratio is of primary importance. Regardless initial metal oxidation states in corresponding salts, crystallographic data illustrated M:L ratios of 1:1 for the dithizone reaction with antimony(III)chloride and 1:2 for reactions with copper(II) and tin(II) chloride salts. Bond length data illustrated how larger metal ionic radii favor stronger M–S bonds while smaller radii favor stronger M–N bonds.

Together, HOMO and LUMO renderings of DFT geometry optimized metal salts correspond to experimental geometries of final products. Calculated electronic and Gibbs free energy changes for all possible ratios in the metal – ligand reactions produced lowest energies in agreement with experimentally observed reaction ratios. Molecular orbital geometry and free energy theoretical calculations therefore serve as accurate predictive tools in dithizone-metal chemistry.

Disclosure statement

No potential conflict of interest was reported by the authors.

Acknowledgements

This work has received support from the Norwegian Supercomputing Program (NOTUR) through a grant of computer time (Grant No. NN4654K) (JC), the South African National Research Foundation (JC, ML), Central Research Fund of the University of the Free State, Bloemfontein (JC, KGvE) and the University of Pretoria (ML).

Supporting Information

The electronic supporting information includes lists of bond distances and angles for crystal structures reported and the optimized coordinates of the DFT calculations. CCDC 1404517-1404519 contains the supplementary crystallographic data for this paper. These data can be obtained free of charge via <http://www.ccdc.cam.ac.uk/conts/retrieving.html> (or from the Cambridge Crystallographic Data Centre, 12, Union Road, Cambridge CB2 1EZ, UK; fax: +44 1223 336033).

References

-
- [1] H. Fischer, *Wiss. Veröffentlich. Siemens-Werken*, **4**, 158 (1925).
 - [2] (a) H.M.N.H. Irving, *CRC Crit. Rev. Anal. Chem.*, **8**, 321 (1980);
(b) H.M.N.H. Irving, *Dithizone*, The Chemical Society, London (1977).
 - [3] J.F. van Staden, R.E. Taljaard, *Talanta*, **64**, 1203 (2004).
 - [4] A.L.D. Comitre, B.F. Reis, *Talanta* at www.sciencedirect.com (2004).
 - [5] (a) K.G. von Eschwege, *J. Photochem. & Photobiol. A*, **252**, 159 (2013).
(b) E. Alabaraoye, K.G. von Eschwege, N. Loganathan, *J. Phys. Chem. A*, **118**, 10894 (2014).
 - [6] (a) H. Schwoerer, K.G. von Eschwege, G. Bosman, P. Krok, J. Conradie, *ChemPhysChem*, **12**, 2653 (2011).
(b) K.G. von Eschwege, G. Bosman, J. Conradie, H. Schwoerer, *J. Phys. Chem. A*, **118**, 844 (2014).
 - [7] (a) K.G. von Eschwege, J. Conradie, J.C. Swarts, *J. Phys. Chem. A*, **112**, 2211 (2008).
(b) K.G. von Eschwege, J. Conradie, A. Kuhn, *J. Phys. Chem. A*, **115**, 14637 (2011).
 - [8] (a) F. Kong, W. Wong, *J. Chem. Soc. Dalton Trans.*, 2497 (1999).
(b) K.G. von Eschwege, J.C. Swarts, M.A.S. Aquino and T.S. Cameron, *Acta Cryst.* **E68**, m1518 (2012).
 - [9] APEX2 (including SAINT and SADABS), Bruker AXS Inc., Madison, WI (2012).

-
- [10] G.M. Sheldrick, *Acta Cryst. A*, **46**, 112 (2008).
- [11] (a) A.D. Becke, *Phys. Rev. A*, **38**, 3098 (1988).
(b) C.T. Lee, W.T. Yang, R.G. Parr, *Phys. Rev. B*, **37**, 785 (1988).
- [12] M.J. Frisch, G.W. Trucks, H.B. Schlegel, G.E. Scuseria, M.A. Robb, J.R. Cheeseman, G. Scalmani, V. Barone, B. Mennucci, G.A. Petersson, H. Nakatsuji, M. Caricato, X. Li, H.P. Hratchian, A.F. Izmaylov, J. Bloino, G. Zheng, J.L. Sonnenberg, M. Hada, M. Ehara, K. Toyota, R. Fukuda, J. Hasegawa, M. Ishida, T. Nakajima, Y. Honda, O. Kitao, H. Nakai, T. Vreven, J.A. Montgomery (Jr), J.E. Peralta, F. Ogliaro, M. Bearpark, J.J. Heyd, E. Brothers, K.N. Kudin, V.N. Staroverov, T. Keith, R. Kobayashi, J. Normand, K. Raghavachari, A. Rendell, J.C. Burant, S.S. Iyengar, J. Tomasi, M. Cossi, N. Rega, J.M. Millam, M. Klene, J.E. Knox, J.B. Cross, V. Bakken, C. Adamo, J. Jaramillo, R. Gomperts, R.E. Stratmann, O. Yazyev, A.J. Austin, R. Cammi, C. Pomelli, J.W. Ochterski, R.L. Martin, K. Morokuma, V.G. Zakrzewski, G.A. Voth, P. Salvador, J.J. Dannenberg, S. Dapprich, A.D. Daniels, O. Farkas, J.B. Foresman, J.V. Ortiz, J. Cioslowski, D.J. Fox, Gaussian 09, Revision D.01, Gaussian Inc., Wallingford CT (2010).
- [13] F. Weigend, R. Ahlrichs, *PhysChemChemPhys*, **7**, 3297 (2005).
- [14] J.P. Perdew, J.A. Chevary, S.H. Vosko, K.A. Jackson, M.R. Pederson, D.J. Singh, C. Fiolhais, *Phys. Rev. B*, **46** (1992) 6671. Erratum: J.P. Perdew, J.A. Chevary, S.H. Vosko, K.A. Jackson, M.R. Pederson, D.J. Singh, C. Fiolhais, *Phys. Rev. B*, **48**, 4978 (1993).
- [15] ADF2013, SCM, Theoretical Chemistry, Vrije Universiteit, Amsterdam, The Netherlands, The ADF program system uses methods described in: G. te Velde, F. M. Bickelhaupt, E. J. Baerends, C. F. Guerra, S. J. A. van Gisbergen, J. G. Snijders, T. Ziegler, *J. Comput. Chem.*, **22**, 931 (2001).
- [16] L.J. Farrugia, *J. Appl. Cryst.*, **45**, 849 (2012).
- [17] B. Knopf, *Proc. Chem. Soc.*, London, 203 (1961) (CCDC: ZZZEDU).
- [18] M. Laing, P. Sommerville, P.A. Alsop, *J. Chem. Soc. A*, 1247 (1971).
- [19] A. Mawby, H.M.N.H. Irving, *J. Inorg. Nucl. Chem.*, **34**, 109 (1972).
- [20] J.A. Lessa, D.C. Reis, I.C. Mendes, N.L. Speziali, L.F. Rocha, V.R.A. Pereira, C.M.L. Melo, H. Beraldo, *Polyhedron*, **30**, 372 (2011).
- [21] (a) R. Zhang, F. Li, C. Ma, *Indian J. Chem. Sect. A*, **43**, 1109 (2004);
(b) J.A.D. Delgado, C.K.Y.A. Okio, R. Welter, *Acta Cryst. E*, **65**, m426 (2009);
(c) C. Ma, F. Li, R. Zhang, H. Yin, *Chin. J. Org. Chem.*, **23**, 595 (2003).
- [22] K. Ortner, U. Abram, *Polyhedron*, **18**, 749 (1999).
- [23] M.L. Niven, H.M.N.H. Irving, L.R. Nassimbeni, A.T. Hutton, *Acta Cryst. B*, **38**, 2140 (1982).
- [24] K.G. von Eschwege, L. van As, C.C. Joubert, J.C. Swarts, M.A.S. Aquino, T.S. Cameron, *Electrochim. Acta*, **112**, 747 (2013).
- [25] (a) A.T. Hutton, H.M.N.H. Irving, L.R. Nassimbeni, G. Gafner, *Acta Cryst. B*, **36**, 2064 (1980);
(b) K.G. von Eschwege, F. Muller, A. Muller, *Acta Cryst. E*, **67**, m1804 (2011);
(c) K.G. von Eschwege, F. Muller, A. Muller, *Acta Cryst. E*, **67**, m1858 (2011).
- [26] J.McB. Harrowfield, C. Pakawatchai, A.H. White, *J. Chem. Soc. Dalton Trans.*, 1109 (1983).

-
- [27] G. Seamans, J.L. Walsh, M. Krawiec, W.T. Pennington, *Acta Cryst. C*, **59**, m268 (2003).
- [28] C. Ma, F. Li, R. Zhang, H. Yin, Y. Huaxue, *Chin. J. Org. Chem.* **23**, 595 (2003).
- [29] R. Zhang, F. Li, C. Ma, *Indian J. Chem. A*, **43**, 1109 (2004).
- [30] A. Irving, H.M.N.H. Irving, *J. Cryst. Spec. Res.*, **16**, 495 (1986).
- [31] A.A. Pasynskii, A.V. Romanenkov, Yu.V. Torubayev, P.V. Belousov, K.A. Lyssenko, *Zh. Neorg. Khim. Russ. J. Inorg. Chem.*, **47**, 2004 (2002).
- [32] (a) M. Winter, Web Elements Ltd, UK, University of Sheffield (2015);
(b) R.D. Shannon, *Acta Cryst. A*, **32**, 751 (1976).
- [33] P.C. Burns, F.C. Hawthorne, *American Mineralogist*, **78**, 187 (1993).